Analysis of double-scattering mechanisms in $\bar{p}d$ annihilation processes between 1.09 and 1.43 GeV/c

P. D. Zemany,* J. M. Mountz,† and Z. Ming Ma
Department of Physics, Michigan State University, East Lansing, Michigan 48824
(Received 24 October 1979; revised manuscript received 5 September 1980)

In a study of $\bar{p}d$ annihilation reactions between 1.09 and 1.43 GeV/c, it is found that the four- and six-prong samples with a visible slow proton exhibit features substantially different from those expected based on a simple impulse approximation. A phenomenological model, developed in the framework of Glauber's model, provides an excellent description of the data. In as much as 26.6% of the three- and four-prong and 21.7% of the five- and six-prong samples, pions from one of the annihilation reactions interact with the spectator nucleon via either elastic or charge-exchange scattering. This process is called the final-state interaction. For the initial-state interaction in which the incident antiproton undergoes elastic scattering prior to annihilation, the process accounts for 7.5% (9.1%) of the three- and four- (five- and six-) prong events.

I. INTRODUCTION

The use of a deuteron target as a source of free neutrons has long been standard practice in high-energy physics. Owing to the fact that a deuteron is a loosely bound state of a proton and a neutron with a binding energy of only 2.2 MeV, one may naively assume that the deuteron breaks up spontaneously upon impact by the projectile particle. Such a picture was found to be inconsistent with experimental data. In reactions, such as pd and $\pi^{\pm}d$, where cross sections for the projectile particle with a proton are known, and those with a neutron can be inferred through charge independence, experimental data are inconsistent with the notion that cross sections with a deuteron target are sir ple sums of those with a proton and a neutron target. This cross-section defect was explained in terms of nuclear shadowing in an elegant theory proposed by Glauber[1] and by Glauber and Franco.[2,3] The theory was modified later to include isospin-exchange effects[4] and the effect of deuteron quadrupole deformation[5,6] on the scattering amplitude. Although the Glauber model provides a precise recipe for elastic and simple deuteron-breakup reactions, i.e.,

$$hd \to hd \tag{1}$$

and

$$hd \to hpn\,, \tag{2}$$

where h is the incident particle, and the model has been found to agree well with data for the incident antiproton[7] and proton,[8] no simple description is available for reactions in which particle production or annihilation processes occur. Although there is abundant experimental evidence in pd (Ref. 9), $\pi^{\pm}d$ (Ref. 10), $K^{\pm}d$ (Ref. 11), and $\bar{p}d$ (Ref. 12) reactions for multiple scattering inside the deuteron, no thorough and complete phenomenological analysis of these has been reported. This is primarily due to the complexity of the double-scattering mechanisms present in the high-energy scattering.

In this paper, a definitive study of double-scattering processes in $\bar{p}n$-like annihilation reactions is presented. An abbreviated version of this work has been published previously.[13] Data for this work came from an exposure of the Brookhaven National Laboratory 31-in. deuterium bubble chamber by a separated $\bar{p}$ beam. A total of 150 000 triads were taken, with 64 000 triads at 1.31 GeV/c and the remaining roughly evenly divided among 1.09, 1.19, and 1.43 GeV/c. Events analyzed in this work are from the reactions

$$\bar{p}d \to p + 2\pi^- + \pi^+ + j\pi^0, \quad j \geq 0\,, \tag{3}$$

$$\to p + 3\pi^- + 2\pi^+ + j\pi^0, \quad j \geq 0\,. \tag{4}$$

Details of this experiment are given elsewhere.[14]

II. EVIDENCE FOR DOUBLE SCATTERING

If the idea is indeed correct that the deuteron breakup occurs spontaneously when the incident particle interacts with one of the constituent nucleons, characteristic features of the spectator nucleon may be predicted using deuteron wave functions. This process will be referred to as the impulse approximation. Figure 1(a) shows the expected internal Fermi-momentum distribution of the constituent nucleons using the Reid soft-core wave function.[15] In comparison, the momentum distributions of protons emerging from apparent $\bar{p}n$ annihilations in a deuterium target are shown in Figs. 1(b) and 1(c) for reactions (3) and (4), respectively. One notes that protons having a momentum less than 70 MeV do not produce observable tracks in liquid hydrogen and, hence, are not detected in a bubble chamber. Even protons having a momentum between 70 and 130 MeV/c are

systematically lost. By comparing the data to the impulse-approximation prediction above 130 MeV/c, a region of apparent excess may be observed. This excess appears to be in the form of a broad peak or bump centered at 300 MeV/c. Similarly, this excess is present when the data are compared with other deuteron wave functions.[16-20]

The probability of neutron-proton separation r is given by $\phi^2(r)r^2$, where $\phi(r)$ is the deuteron radial-wave function. This function has a maximum at $r \simeq 2$ fm. Since the nucleon dimensions are of the order of one fermi, it is not difficult to accept that both nucleons may be involved in a scattering process. Two possible ways the proton could be involved are depicted in Fig. 2. The first diagram (called final-state interaction or FSI) describes a pion, from the $\bar{p}n$ annihilation, interacting with the spectator proton. The second is called initial-state interaction or ISI. Here, the antiproton scatters from the proton before $\bar{p}n$ annihilation takes place. The presence of FSI and ISI is evidenced by features characteristic of these processes.

Since FSI results when a pion scatters from the spectator nucleon, production of the $\Delta(1236)$ resonance is expected. Figures 3(a) and 3(b) show the π^+p invariant-mass distributions from four- and six-prong topologies, respectively. For comparison, the π^-p distributions, normalized to the corresponding π^+p distributions, are shown shaded. Only events with spectator momenta above 190 MeV/c were used in these plots. A peak in the π^+p mass distributions characteristic of the $\Delta(1236)$ resonance is apparent. Although both π^- and π^+ may scatter from the spectator proton, owing to the fact that the π^-p cross section is smaller than the π^+p cross section in the $\Delta(1236)$ region, one expects a more copious production of $\Delta(1236)$ in the π^+p than in π^-p mass distributions. In addition, there is one more π^- than π^+ in an event. Assuming that only one of the pions scatters from the proton, enhancements in the π^-p mass distribution are expected to be more diluted than those in the π^+p mass distribution.

The ISI process results when the antiproton elastically scatters from one of the constituent

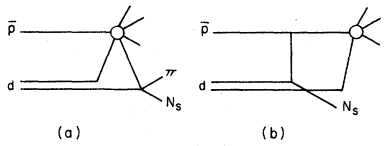

FIG. 2. (a) Final-state interaction. (b) Initial-state interaction.

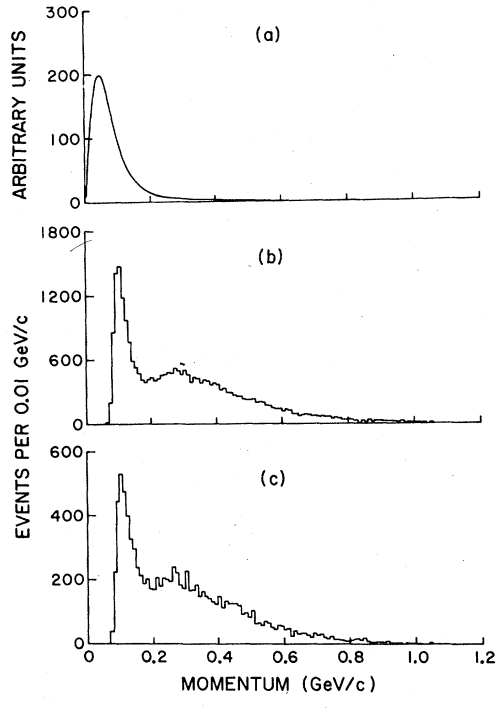

FIG. 1. (a) Expected spectator-nucleon-momentum distribution. (b) and (c) Observed momentum distributions of the final-state proton for four- and six-prong topologies, respectively.

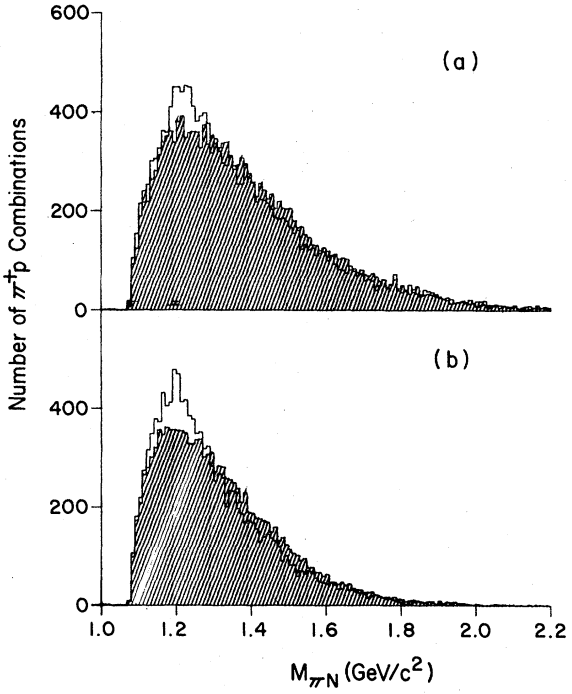

FIG. 3. π^+p (unshaded) invariant-mass distribution compared with that of π^-p (shaded) for (a) four-prong and (b) six-prong data. The π^-p distributions have been normalized to the respective π^+p distributions. A cut for $P_p \geq 190$ MeV/c has been made.

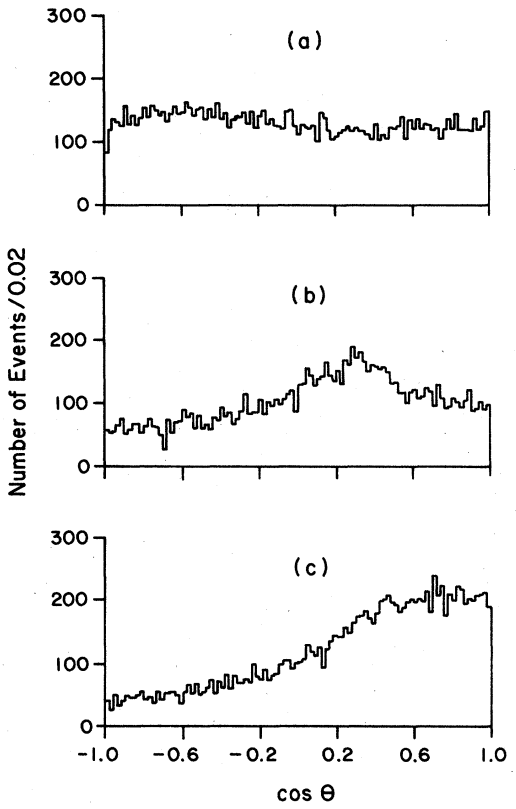

FIG. 4. Proton laboratory angular distribution for (a) $P_p \leq 190$ MeV/c, (b) $190 < P_p \leq 350$ MeV/c, and (c) $P_p > 350$ MeV/c.

nucleons before being annihilated by the other. The elastic scattering imparts a transverse momentum to the spectator nucleon. Therefore, the laboratory angular distribution of the spectator nucleon with respect to the beam is expected to exhibit a bump characteristic of elastic scattering. Figure 4 shows the spectator cosine distribution for three spectator-momentum ranges. For $p_p < 190$ MeV/c, the data shown in Fig. 4(a) appear to be smooth. A peak at $\cos\theta$ between 0.2 and 0.4 is seen for spectator momenta in the range 190–350 MeV/c as is shown in Fig. 4(b). This peak persists for spectator momenta greater than 350 MeV/c as may be seen in Fig. 4(c). In contrast, the angular distribution of a spectator proton is expected to be a monotonically increasing function in $\cos\theta$, in a simple impulse model.

In summary, characteristics of the protons emerging from apparent $\bar{p}n$-like annihilation show significant deviation from those predicted by a simple impulse approximation. Although effects attributable to FSI processes have been observed previously[21,22] no comprehensive descriptions of either the FSI or the ISI process have been reported. In the following sections, a phenomenological model in the spirit of the Glauber model is developed to provide a comprehensive picture of the double-scattering mechanisms present in the data. It is worth noting that unlike other previously reported studies of double-scattering effects, there is only one final-state nucleon in the $\bar{p}d$ annihilation data. Therefore, effects due to possible confusion and misidentification of the spectator nucleon do not exist.

III. FINAL-STATE INTERACTION

Using a simple geometric picture, the probability that a pion from the annihilation will interact with the spectator nucleon may be estimated by

$$\mathcal{P} = \frac{\sigma_{\pi N}}{4\pi}\left\langle \frac{1}{r^2} \right\rangle, \tag{5}$$

where $\langle 1/r^2 \rangle$ is the mean-inverse-square neutron-proton separation in the deuteron, and $\sigma_{\pi N}$ is the pion-nucleon cross section evaluated at the c.m. energy of the pion-spectator nucleon system. Using values of ~0.25 fm^{-2} for $\langle 1/r^2 \rangle$ and ~60 mb for $\sigma_{\pi N}$ one gets a probability of 12%. Assuming that the πN scattering amplitude is independent of r, the FSI amplitude may be written simply as

$$F(r) \sim f_{\pi N}\frac{\phi(r)}{r}, \tag{6}$$

where $\phi(r)$ is the deuteron S-wave radial wave function, and $f_{\pi N}$ is the πN scattering amplitude. Fourier transformed, the FSI amplitude in the momentum space is given by

$$f(p) = Cf_{\pi N}\int \frac{\phi(r)}{r} e^{-ip\cdot r} d^3r \tag{7}$$

TABLE I. Percentage contributions to FSI processes by elastic and inelastic πN scattering.

Topology	Four prong		Six prong	
	π^+p	π^-p	π^+p	π^-p
Elastic/charge-exchange processes	94%	85%	97%	91%
Inelastic processes	6%	15%	3%	9%

$$= Cf_{\pi N} g(p), \tag{8}$$

where C is a normalization constant. The probability for FSI in momentum space is therefore given by

$$P(p) = 4C^2 \sigma_{\pi N} g^2(p) p^2. \tag{9}$$

Owing to the limited invariant phase space of the pion-nucleon system available in this experiment, the potential contributions due to particle-production reactions are expected to be small. Consider the integrals

$$I_{el} = \int \sigma_{el}(\pi N_s) \frac{d\vec{p}}{E}, \tag{10}$$

$$I_{in} = \int \sigma_{in}(\pi N_s) \frac{d\vec{p}}{E}, \tag{11}$$

where $\sigma_{el}(\pi N_s)$ and $\sigma_{in}(\pi N_s)$ are the elastic/charge exchange and inelastic parts of the total pion-nucleon cross section, respectively, and the factor $d\vec{p}/E$ is the invariant phase space of the pion-nucleon systems in the double-scattering process. Using the Fermi-momentum distribution of the constituent nucleon, $\phi^2(p)p^2$ as is prescribed by the impulse approximation, and the momentum distribution of the pions from the annihilation given by Fermi's statistical model,[23] the resultant contribution to the FSI due to particle-production processes is shown in Table I. It ranges from 3 to 6% for π^+ and 9 to 15% for π^-. In this work, only elastic and two-body charge-exchange amplitudes are used in evaluating the πN-scattering cross sections.

Table II lists $\bar{p}n$-like annihilation channels with up to seven pions that are potentially present in the data sample. Events with a proton in the final state are described as belonging to the $\bar{p}n$-like topology. A total of 23 reactions were considered with fourteen for the three- or four-prong topologies and nine for the five- or six-prong topologies. Since a proton may result from a spectator-neutron charge-exchange scattering on a pion from the $\bar{p}p$ annihilation, many of these $\bar{p}n$-like events may actually be examples of $\bar{p}p$ annihilation. Conversely, charge-exchange scattering can also cause $\bar{p}n$ annihilation events to have a topology characteristic of $\bar{p}p$ annihilations. These events are missing from the sample.

To model the effects of FSI, examples of $\bar{p}n$ and $\bar{p}p$ annihilation were generated for each reaction listed in Table II according to Fermi's statistical model. Reaction cross sections for $\bar{p}n$ interactions in this momentum range involving less than two missing neutral particles are determined and may be found elsewhere.[24] Those for the $\bar{p}p$ annihilations were obtained from published re-

TABLE II. Contributing terms to FSI processes.

Reaction	πN_s scattering process	Remark
$\bar{p}d \to p_s \pi^+ 2\pi^- j\pi^0$, $j=0,1,2,3,4$	$\pi^+ p$, $\pi^- p$, $\pi^0 p$ elastics $\pi^- p \to \pi^0 n$, $\pi^0 p \to \pi^+ n$	$\bar{p}n$ annihilation, properly counted $\bar{p}n$ annihilation, leaving $\bar{p}n$ topology
$\bar{p}d \to n_s 2\pi^+ 2\pi^- j\pi^0$, $j=0,1,2,3$	$\pi^+ n$, $\pi^- n$, $\pi^0 n$ elastics $\pi^+ n \to \pi^0 p$ $\pi^0 n \to \pi^- p$	$\bar{p}p$ annihilation, properly counted $\bar{p}p$ annihilation, leaving $\bar{p}p$ topology into $\bar{p}n$ three- and four-prong topology $\bar{p}p$ annihilation, leaving $\bar{p}p$ topology into $\bar{p}n$ five- and six prong topology
$\bar{p}d \to n_s \pi^+ \pi^- j\pi^0$, $j=1,2,3,4,5$	$\pi^+ n$, $\pi^- n$, $\pi^0 n$ elastics $\pi^+ n \to \pi^0 p$ $\pi^0 n \to \pi^- p$	$\bar{p}p$ annihilation, properly counted $\bar{p}p$ annihilation, leaving $\bar{p}p$ topology into $\bar{p}n$ one- and two-prong topology $\bar{p}p$ annihilation, leaving $\bar{p}p$ topology into $\bar{p}n$ three- and four-prong topology
$\bar{p}d \to p_s 2\pi^+ 3\pi^- j\pi^0$, $j=0,1,2$	$\pi^+ p$, $\pi^- p$, $\pi^0 p$ elastics $\pi^- p \to \pi^0 n$, $\pi^0 p \to \pi^+ n$	$\bar{p}n$ annihilation, properly counted $\bar{p}n$ annihilation, leaving $\bar{p}n$ topology
$\bar{p}d \to n_s 3\pi^+ 3\pi^- j\pi^0$, $j=0,1$	$\pi^+ n$, $\pi^- n$, $\pi^0 n$ elastics $\pi^+ n$, $\to \pi^0 p$ $\pi^0 n \to \pi^- p$	$\bar{p}p$ annihilation, properly counted $\bar{p}p$ annihilation, leaving $\bar{p}p$ topology into $\bar{p}n$ five- and six- prong topology $\bar{p}p$ annihilation, leaving $\bar{p}p$ topology into $\bar{p}n$ seven- and eight-prong topology
$\bar{p}d \to n_s 2\pi^+ 2\pi^- j\pi^0$, $j=1,2,3$	$\pi^+ n$, $\pi^- n$, $\pi^0 n$ elastics $\pi^+ n \to \pi^0 p$ $\pi^0 n \to \pi^- p$	$\bar{p}p$ annihilation, properly counted $\bar{p}p$ annihilation, leaving $\bar{p}p$ topology into $\bar{p}n$ three- and four-prong topology $\bar{p}p$ annihilation, leaving $\bar{p}p$ topology into $\bar{p}n$ five- and six-prong topology

ports.[25-30] Cross sections for the reactions involving two or more π^0 in the final state were not directly measured. These are calculated using Fermi's statistical model. The model has been shown to be in good agreement with $\bar{p}N$ annihilations[31] in this momentum range. Neglecting pion-mass difference, the model relates cross sections for pion production as follows:

$$\sigma_r = \frac{n_0^i! n_-^i! n_+^i!}{n_0^r! n_-^r! n_+^r!} \sigma_i \tag{12}$$

and

$$n_0^r + n_-^r + n_+^r = n_0^i + n_-^i + n_+^i , \tag{13}$$

where n_0^r, n_-^r, and n_+^r denote, respectively, the numbers of π^0, π^-, and π^+ produced in the rth reaction. Similarly, for the ith channel, the numbers of π^0, π^-, and π^+ produced are given by n_0^i, n_-^i, and n_+^i, respectively. The cross-section values used in the calculation are listed in Table III. The constituent proton and neutron are assumed to have equal but opposite momenta given by the distribution function $\phi^2(p)p^2$. The constituent nucleons as well as pions from the annihilation processes are assumed to be on the mass shell. Each generated event is weighted by an appropriate flux factor to account for the Fermi motion of the target and by the pion-nucleon cross section calculated from the phase-shift results of Donnachie, Kirsopp, and Lovelace.[32] Kinematics of the outgoing pion and nucleon is assumed to be given also by the same phase-shift results. Characteristic features of the FSI process are shown in Figs. 5(d)–5(f) [Figs. 6(d)–6(f)] for three- and four-prong [five- and six-prong] topologies, respectively. An enhancement at $\Delta(1236)$, although diluted by combinatorial ambiguities, is evident in the π^+p mass distribution. The most subtle effect of FSI is due to the charge-

TABLE III. $\bar{p}p$ and $\bar{p}n$ cross sections.

Reaction	1.09 GeV/c	1.19 GeV/c	1.31 GeV/c	1.43 GeV/c
$\bar{p}n \to 2\pi^-\pi^+$	2.17 ± 0.17	1.81 ± 0.13	1.61 ± 0.09	1.42 ± 0.10
$\bar{p}n \to 2\pi^-\pi^+\pi^0$	11.43 ± 0.53	10.96 ± 0.45	9.41 ± 0.33	8.89 ± 0.35
[a] $\bar{p}n \to 2\pi^-\pi^+2\pi^0$	12.3 ± 0.9	12.1 ± 0.7	11.1 ± 0.6	10.1 ± 0.6
[a] $\bar{p}n \to 2\pi^-\pi^+3\pi^0$	6.9 ± 0.4	6.5 ± 0.3	6.7 ± 0.3	6.2 ± 0.3
[a] $\bar{p}n \to 2\pi^-\pi^+4\pi^0$	2.4	2.5	2.6	2.6
$\bar{p}n \to 3\pi^-2\pi^+$	4.10 ± 0.26	4.02 ± 0.22	3.70 ± 0.17	3.38 ± 0.17
$\bar{p}n \to 3\pi^-2\pi^+\pi^0$	6.85 ± 0.37	6.46 ± 0.29	6.74 ± 0.24	6.24 ± 0.27
$\bar{p}n \to 3\pi^+2\pi^-\pi^0 + \mathrm{MM}$	4.84 ± 0.28	5.01 ± 0.24	5.14 ± 0.21	5.18 ± 0.24
[b] $\bar{p}p \to 2\pi^+2\pi^-$	3.6 ± 0.2	3.3 ± 0.2	3.0 ± 0.2	2.8 ± 0.2
[b] $\bar{p}p \to 2\pi^+2\pi^-\pi^0$	13.5 ± 1.5	12.9 ± 1.3	12.0 ± 1.2	11.1 ± 1.0
[a] $\bar{p}p \to 2\pi^+2\pi^-2\pi^0$	4.5	5.0	5.4	5.4
[a] $\bar{p}p \to 2\pi^+2\pi^-3\pi^0$	3.3	3.3	3.3	3.3
[b] $\bar{p}p \to 2\pi^+2\pi^- + \mathrm{MM}$	11.4 ± 0.5	11.2 ± 0.5	11.0 ± 0.5	10.9 ± 0.5
[b] $\bar{p}p \to 3\pi^+3\pi^-$	1.0	1.1	1.2	1.2
[b] $\bar{p}p \to 3\pi^+3\pi^-\pi^0$	2.2	2.2	2.2	2.2
[b] $\bar{p}p \to 3\pi^+3\pi^- + \mathrm{MM}$	0.3 ± 0.2	0.3 ± 0.2	0.4 ± 0.2	0.5 ± 0.3
[b] $\bar{p}p \to \pi^+\pi^-\pi^0$	2.2	1.8	1.6	1.4
[a] $\bar{p}p \to \pi^+\pi^-2\pi^0$	7.2	6.6	6.0	5.6
[a] $\bar{p}p \to \pi^+\pi^-3\pi^0$	9.0	8.6	8.0	7.4
[a] $\bar{p}p \to \pi^+\pi^-4\pi^0$	1.5	1.7	1.8	1.8
[a] $\bar{p}p \to \pi^+\pi^-5\pi^0$	0.7	0.7	0.7	0.7
[b] $\bar{p}p \to \pi^+\pi^- + \mathrm{MM}$	18.8 ± 0.7	18.0 ± 0.1[b]	16.8 ± 0.6[b]	15.8 ± 0.6

[a] Calculated from Eq. (9).
[b] Taken from references (see text).

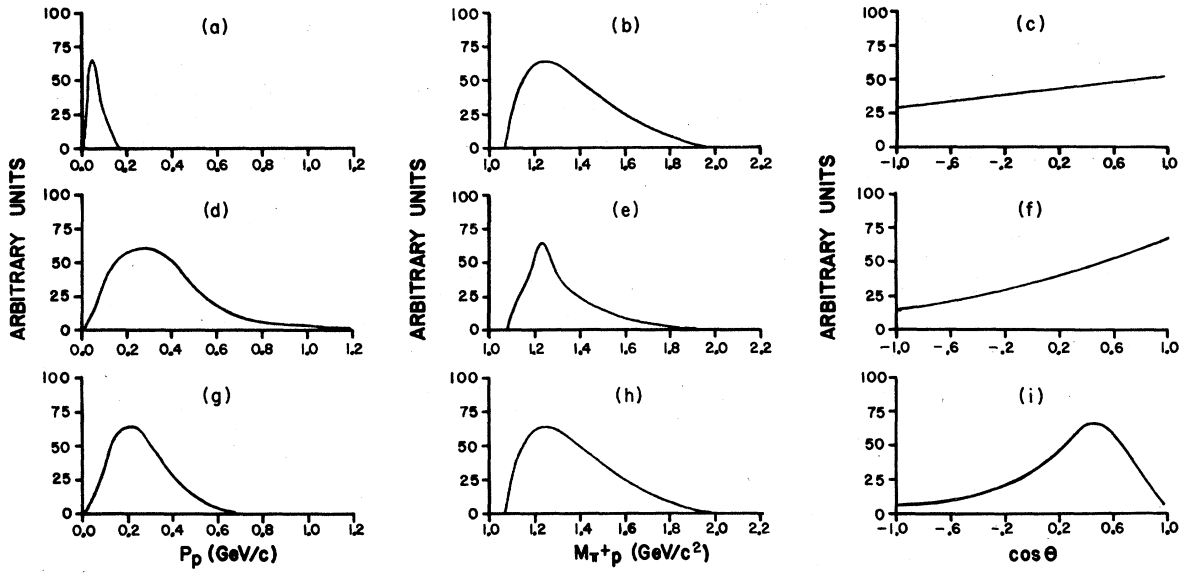

FIG. 5. Characteristic distributions of proton in the three- and four-prong topologies. (a)–(c) Model prediction for single-scattering events, i.e., impulse approximation modified to exclude double-scattering-effected events. (d)–(f) Model prediction for the FSI process. (g)–(i) Model prediction for the ISI process.

exchange process, i.e., a $\bar{p}n$ annihilation event may lose the accompanying proton spectator through FSI and appear in the $\bar{p}p$-like topology. Similar misidentification may also occur to $\bar{p}p$ annihilation events. The reaction-dependent probabilities of FSI and related topology-changing effects are given in Tables IV–VII. As may be expected, the probability of FSI increases with a greater number of pions from the annihilation. The model predicts a probability of ~8% for the $\bar{p}n \to \pi^+\pi^-\pi^-$ channel to almost 38% for the $2\pi^+3\pi^-2\pi^0$ channel. These results are summarized in Table VIII. A significant fraction, between $\frac{1}{3}$ and $\frac{1}{4}$, of these FSI-effected events is expected to change

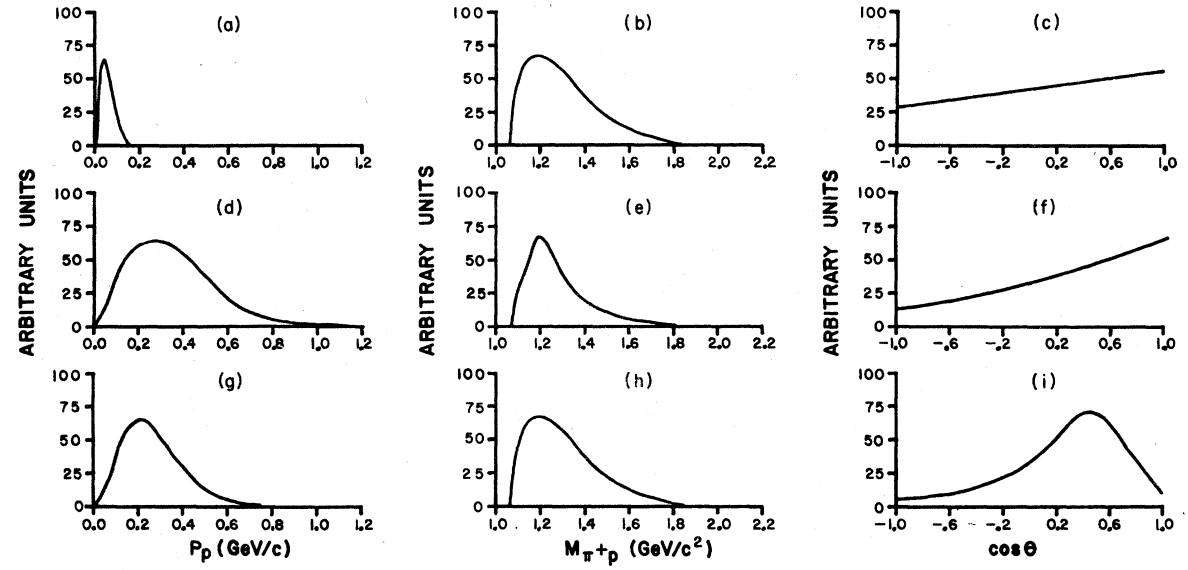

FIG. 6. Characteristic distributions of proton in the five- and six-prong topologies. (a)–(c) Model prediction for single-scattering events, i.e., impulse approximation modified to exclude double-scattering-effected events. (d)–(f) Model prediction for the FSI process. (g)–(i) Model prediction for the ISI process.

TABLE IV. Predicted channel-dependent FSI probabilities at 1.09 GeV/c.

Reaction	$\bar{p}n$ FSI	$\bar{p}n$ FSI leaving $\bar{p}n$ topology	$\bar{p}p$ FSI entering $\bar{p}n$ topology	$\bar{p}n$-like topology
$\bar{p}p \to 2\pi^+2\pi^-$			0.041	4
$\bar{p}p \to 2\pi^+2\pi^-\pi^0$			0.046	4
$\bar{p}p \to 2\pi^+2\pi^-\pi^0$			0.067	4
$\bar{p}p \to 2\pi^+2\pi^-3\pi^0$			0.062	4
$\bar{p}p \to \pi^+\pi^-\pi^0$			0.014	4
$\bar{p}p \to \pi^+\pi^-2\pi^0$			0.040	4
$\bar{p}p \to \pi^+\pi^-3\pi^0$			0.073	4
$\bar{p}p \to \pi^+\pi^-4\pi^0$			0.122	4
$\bar{p}p \to \pi^+\pi^-5\pi^0$			0.134	4
$\bar{p}n \to \pi^+2\pi^-$	0.090	0.030		4
$\bar{p}n \to \pi^+2\pi^-\pi^0$	0.151	0.059		4
$\bar{p}n \to \pi^+2\pi^-2\pi^0$	0.207	0.095		4
$\bar{p}n \to \pi^+2\pi^-3\pi^0$	0.280	0.172		4
$\bar{p}n \to \pi^+2\pi^-4\pi^0$	0.340	0.165		4
$\bar{p}p \to 3\pi^+3\pi^-$			0.085	6
$\bar{p}p \to 3\pi^+3\pi^-\pi^0$			0.086	6
$\bar{p}p \to 2\pi^+2\pi^-\pi^0$			0.027	6
$\bar{p}p \to 2\pi^+2\pi^-2\pi^0$			0.055	6
$\bar{p}p \to 2\pi^+2\pi^-3\pi^0$			0.079	6
$\bar{p}n \to 2\pi^+3\pi^-$	0.239	0.075		6
$\bar{p}n \to 2\pi^+3\pi^-\pi^0$	0.306	0.125		6
$\bar{p}n \to 2\pi^+3\pi^-2\pi^0$	0.375	0.149		6

topological appearance due to charge-exchange scattering.

IV. INITIAL-STATE INTERACTION

In the ISI process, the incident antiproton scatters elastically from one of the constituent nucleons before annihilating with another. At the initial-scattering vertex, the proton acquires a transverse momentum. The process is parametrized by $d\sigma/d\Omega = (d\sigma/d\Omega)_0 e^{-At}$, where $A = 17.5$ GeV^{-2} and the total elastic cross section is 42 mb (Refs. 29 and 30) in the momentum range used here.

TABLE V. Predicted channel-dependent FSI probabilities at 1.19 GeV/c.

Reaction	$\bar{p}n$ FSI	$\bar{p}n$ FSI leaving $\bar{p}n$ topology	$\bar{p}n$ FSI entering $\bar{p}n$ topology	$\bar{p}n$-like topology
$\bar{p}p \to 2\pi^+2\pi^-$			0.039	4
$\bar{p}p \to 2\pi^+2\pi^-\pi^0$			0.045	4
$\bar{p}p \to 2\pi^+2\pi^-2\pi^0$			0.051	4
$\bar{p}p \to 2\pi^+2\pi^-3\pi^0$			0.061	4
$\bar{p}p \to \pi^+\pi^-\pi^0$			0.014	4
$\bar{p}p \to \pi^+\pi^-2\pi^0$			0.040	4
$\bar{p}p \to \pi^+\pi^-3\pi^0$			0.074	4
$\bar{p}p \to \pi^+\pi^-4\pi^0$			0.123	4
$\bar{p}p \to \pi^+\pi^-5\pi^0$			0.133	4
$\bar{p}n \to \pi^+2\pi^-$	0.089	0.031		4
$\bar{p}n \to \pi^+2\pi^-\pi^0$	0.149	0.059		4
$\bar{p}n \to \pi^+2\pi^-2\pi^0$	0.205	0.095		4
$\bar{p}n \to \pi^+2\pi^-3\pi^0$	0.285	0.151		4
$\bar{p}n \to \pi^+2\pi^-4\pi^0$	0.356	0.160		4
$\bar{p}p \to 3\pi^+3\pi^-$			0.083	6
$\bar{p}p \to 3\pi^+3\pi^-\pi^0$			0.086	6
$\bar{p}p \to 2\pi^+2\pi^-\pi^0$			0.026	6
$\bar{p}p \to 2\pi^+2\pi^-2\pi^0$			0.055	6
$\bar{p}p \to 2\pi^+2\pi^-3\pi^0$			0.080	6
$\bar{p}n \to 2\pi^+3\pi^-$	0.240	0.076		6
$\bar{p}n \to 2\pi^+3\pi^-\pi^0$	0.307	0.120		6
$\bar{p}n \to 2\pi^+3\pi^-2\pi^0$	0.372	0.146		6

TABLE VI. Predicted channel-dependent FSI probabilities at 1.31 GeV/c.

Reaction	$\bar{p}n$ FSI	$\bar{p}n$ FSI leaving $\bar{p}n$ topology	$\bar{p}p$ FSI entering $\bar{p}n$ topology	$\bar{p}n$-like topology
$\bar{p}p \to 2\pi^+2\pi^-$			0.039	4
$\bar{p}p \to 2\pi^+2\pi^-\pi^0$			0.044	4
$\bar{p}p \to 2\pi^+2\pi^-2\pi^0$			0.058	4
$\bar{p}p \to 2\pi^+2\pi^-3\pi^0$			0.058	4
$\bar{p}p \to \pi^+\pi^-\pi^0$			0.013	4
$\bar{p}p \to \pi^+\pi^-2\pi^0$			0.037	4
$\bar{p}p \to \pi^+\pi^-3\pi^0$			0.073	4
$\bar{p}p \to \pi^+\pi^-4\pi^0$			0.100	4
$\bar{p}p \to \pi^+\pi^-5\pi^0$			0.140	4
$\bar{p}n \to \pi^+2\pi^-$	0.087	0.028		4
$\bar{p}n \to \pi^+2\pi^-\pi^0$	0.142	0.058		4
$\bar{p}n \to \pi^+2\pi^-2\pi^0$	0.206	0.098		4
$\bar{p}n \to \pi^+2\pi^-3\pi^0$	0.270	0.150		4
$\bar{p}n \to \pi^+2\pi^-4\pi^0$	0.371	0.172		4
$\bar{p}p \to 3\pi^+3\pi^-$			0.080	6
$\bar{p}p \to 3\pi^+3\pi^-\pi^0$			0.081	6
$\bar{p}p \to 2\pi^+2\pi^-\pi^0$			0.025	6
$\bar{p}p \to 2\pi^+2\pi^-2\pi^0$			0.054	6
$\bar{p}p \to 2\pi^+2\pi^-3\pi^0$			0.078	6
$\bar{p}n \to 2\pi^+3\pi^-$	0.237	0.074		6
$\bar{p}n \to 2\pi^+3\pi^-\pi^0$	0.302	0.115		6
$\bar{p}n \to 2\pi^+3\pi^-2\pi^0$	0.380	0.145		6

Monte Carlo events were generated for $\bar{p}n$ annihilations producing up to seven pions according to the respective cross sections. The energy dependence of the cross section due to the initial elastic scattering of the antiproton is neglected. As is assumed for the FSI process, the Fermi-momentum distribution of the deuteron was given by $\phi^2(p)p^2$. The double-scattering probability was assumed to be proportional to $g^2(p)p^2$. The ISI Monte Carlo events thus generated and weighted were classified according to topologies. Features of ISI-effected events are shown in Figs.

TABLE VII. Predicted channel-dependent FSI probabilities at 1.43 GeV/c.

Reaction	$\bar{p}n$ FSI	$\bar{p}n$ FSI leaving $\bar{p}n$ topology	$\bar{p}p$ FSI entering $\bar{p}n$ topology	$\bar{p}n$-like topology
$\bar{p}p \to 2\pi^+2\pi^-$			0.039	4
$\bar{p}p \to 2\pi^+2\pi^-\pi^0$			0.044	4
$\bar{p}p \to 2\pi^+2\pi^-2\pi^0$			0.065	4
$\bar{p}p \to 2\pi^+2\pi^-3\pi^0$			0.057	4
$\bar{p}p \to \pi^+\pi^-\pi^0$			0.011	4
$\bar{p}p \to \pi^+\pi^-2\pi^0$			0.034	4
$\bar{p}p \to \pi^+\pi^-3\pi^0$			0.071	4
$\bar{p}p \to \pi^+\pi^-4\pi^0$			0.096	4
$\bar{p}p \to \pi^+\pi^-5\pi^0$			0.143	4
$\bar{p}n \to \pi^+2\pi^-$	0.085	0.026		4
$\bar{p}n \to \pi^+2\pi^-\pi^0$	0.135	0.058		4
$\bar{p}n \to \pi^+2\pi^-2\pi^0$	0.204	0.096		4
$\bar{p}n \to \pi^+2\pi^-3\pi^0$	0.266	0.128		4
$\bar{p}n \to \pi^+2\pi^-4\pi^0$	0.365	0.181		4
$\bar{p}p \to 3\pi^+3\pi^-$			0.077	6
$\bar{p}p \to 3\pi^+3\pi^-\pi^0$			0.077	6
$\bar{p}p \to 2\pi^+2\pi^-\pi^0$			0.026	6
$\bar{p}p \to 2\pi^+2\pi^-2\pi^0$			0.052	6
$\bar{p}p \to 2\pi^+2\pi^-3\pi^0$			0.075	6
$\bar{p}n \to 2\pi^+3\pi^-$	0.231	0.069		6
$\bar{p}n \to 2\pi^+3\pi^-\pi^0$	0.295	0.109		6
$\bar{p}n \to 2\pi^+3\pi^-2\pi^0$	0.372	0.145		6

TABLE VIII. Effects of FSI.

	Three, four prongs	Five, six prongs
Fractional amount of FSI with $\bar{p}n$ topology in the data (fitted)	0.266 ± 0.018	0.217 ± 0.015
Fractional amount of fake $\bar{p}n$ events in the data	0.069	0.041
Fraction of $\bar{p}n$ annihilation events lost due to topology changes	0.095	0.062

5(g)–5(i) [Figs. 6(g)–6(i)] for three- and four-prong [five- and six-prong] topologies. As is expected, a characteristic peak at $\cos\theta = 0.4$ can be seen for the proton.

V. SINGLE SCATTERING

Since no qualitative deviation from the impulse model is apparent in the low-spectator-momentum sample, the physics in this region is expected to be simpler. Specifically, for proton momentum below 190 MeV/c, gross features of the spectator proton are expected to be characteristic of impulse approximation. However, the fact that FSI and ISI are more probable for greater internal Fermi momentum causes distortion in the shapes of the spectator distributions of the impulse events. To determine the effect quantitatively, spectator protons with a momentum distribution given by $\phi^2(p)p^2$ were generated. Following the assumption that the probability for double scattering is proportional to $g^2(p)p^2$, the momentum distributions of the impulse-spectator proton are given by those events not involved in double-scattering processes. These are shown in Figs. 5(a)–5(c) [6(a)–6(c)] for three- and four-prong [five- and six-prong] topologies. This remnant group of impulse events are classified as the single-scattering sample. It is apparent that this mechanism does not contribute in the region above 190 MeV/c.

VI. FITS TO THE DATA

To determine quantitatively contributions due to the two double-scattering processes, least-squares fits were made to the data using the $\pi^+ p$ invariant-mass distribution and the momentum and polar angular distributions of the proton. Both the data and Monte Carlo–generated samples include only those events with a proton momentum greater than or equal to 190 MeV/c, the region believed to be dominated by the FSI and ISI processes. It is assumed that no interference exists between the FSI and the ISI processes, i.e., the data distributions are linear sums of those due to FSI and ISI processes,

$$F(p) = BF_{\mathrm{FSI}}(p) + DF_{\mathrm{ISI}}(p)\,, \tag{14}$$

$$C(\cos\theta) = BC_{\mathrm{FSI}}(\cos\theta) + DC_{\mathrm{ISI}}(\cos\theta)\,, \tag{15}$$

$$M(\pi^+ p_s) = BM_{\mathrm{FSI}}(\pi^+ p_s) + DM_{\mathrm{ISI}}(\pi^+ p_s)\,. \tag{16}$$

The Monte Carlo distributions were normalized to unity over the entire spectator-momentum range. Thus the values of the parameters B and D are equal to the numbers of FSI and ISI events in the fitted region, where the proton momentum is greater than or equal to 190 MeV/c. The results are tabulated in Table IX. Since the parameters B and D are independent variables, it is worth noting the excellent agreement obtained in these fits, between the sum of B and D and the actual number of events in the fitted region.

The total number of events in the data sample including both the odd- and even-prong topologies is then given by the sum due to the FSI, ISI, and the modified single-scattering processes. The resulting normalization gives excellent agreement with the data in the 130–190 MeV/c regions of the spectator-momentum distribution. The results

TABLE IX. Summary of fits.

	Three, four prongs	Five, six prongs
Events in fit region ($P_p \geq 190$ MeV/c)	15 891	6188
FSI contribution (B)	12 395 ± 758	4383 ± 307
ISI contribution (D)	3 072 ± 240	1629 ± 184
Total Sample	58 167	25 398
FSI events	15 474 ± 946	5 504 ± 385
Fractional contribution	0.266 ± 0.016	0.217 ± 0.015
ISI events	4 376 ± 341	2 317 ± 262
Fractional contribution	0.075 ± 0.006	0.091 ± 0.010

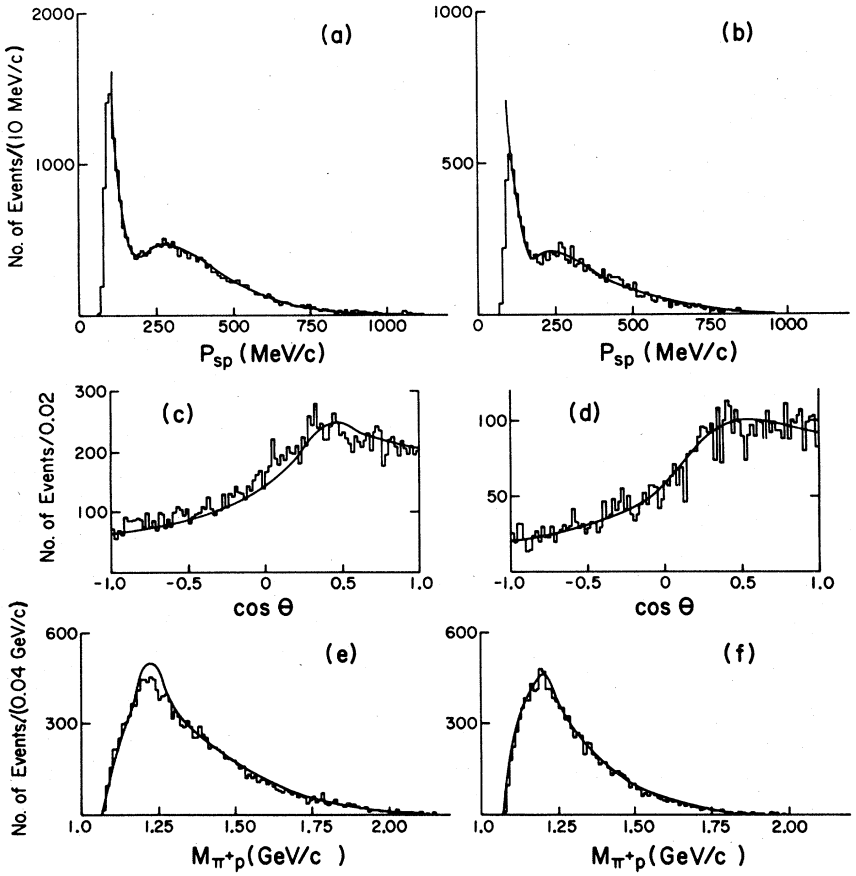

FIG. 7. A comparison of data with the model prediction discussed in the text. (a), (c), and (e) are for four-prong data. (b), (d), and (f) are for six-prong data.

of the fits are summarized in Table IX and shown in Fig. 7 as solid curves. The difference between the numbers of FSI, ISI events and the parameters B, D as determined previously is due to that portion of the proton momentum distributions below 190 MeV/c.

VII. CONCLUSION

In a study of $\bar{p}d$ annihilation reactions between 1.09 and 1.43 GeV/c, it is found that the four- and six-prong samples with a visible, slow proton exhibit features substantially different from those expected based on a simple impulse approximation. In addition to a pronounced excess near 300 MeV/c in the proton momentum distribution, the proton laboratory angular distribution deviates markedly from isotropy. An enhancement is observed at $\cos\theta \simeq 0.4$, indicating that the proton may be a recoil particle from a peripheral collision (referred to as ISI) instead of being a product from a spontaneous impulse breakup. Further evidence for double scattering is seen in the presence of $\Delta^{++}(1236)$ in the invariant mass of the $p\pi^+$ systems, thus indicating scattering of the spectator proton by one of the π^+ from the annihilation processes (referred to as FSI). The evidence for Δ^{++} also suggests that the traditional inference of a neutron target by the presence of a slow proton in the final state may be misleading due to the probability of πN charge-exchange processes.

To quantitatively estimate the contributions in the sample due to the ISI and the FSI processes, a phenomenological model is constructed in the framework of Glauber's model. The model, taking into account FSI, ISI as well as impulse approximation, provides an excellent description of the data with only two free parameters, the percentage contributions due to FSI and ISI processes. For $\bar{p}d$ annihilation reactions between 1.09 and 1.43 GeV/c with a slow proton in the final state, the FSI processes account for 26.6% of the three- and four-prong and 21.7% of the five- and six-prong samples. The corresponding contributions due to the ISI processes are 7.5% (9.1%) for the

three- and four-prong (five- and six-prong) samples.

ACKNOWLEDGMENTS

The authors wish to acknowledge the excellent support provided by the 30- and 31-in. bubble-chamber crew at Brookhaven National Laboratory and the conscientious work by the scanning and measuring staff of MSU. This work was supported in part by National Science Foundation Grant No. PHY 76-01730 and by U. S. Department of Energy Contract No. EG-77-S-02-4529.

*Now at Argonne National Laboratory, Argonne, Illinois 60439.
†Now at School of Medicine, Case–Western Reserve University, Cleveland, Ohio 44106.

[1]R. J. Glauber, Phys. Rev. 100, 242 (1955).
[2]V. Franco and R. J. Glauber, Phys. Rev. 142, 1195 (1966).
[3]R. J. Glauber and V. Franco, Phys. Rev. 156, 1685 (1967).
[4]C. Wilkin, Phys. Rev. Lett. 17, 561 (1966).
[5]V. Franco and R. J. Glauber, Phys. Rev. Lett. 22, 370 (1969).
[6]D. Harrington, Phys. Rev. Lett. 21, 1496 (1968).
[7]Z. Ming Ma and G. A. Smith, Phys. Rev. Lett. 27, 344 (1971).
[8]J. L. Friedes *et al.*, Phys. Rev. Lett. 24, 677 (1970).
[9]J. Hanlon *et al.*, Phys. Rev. D 19, 49 (1979); T. Dombeck *et al.*, *ibid.* 18, 86 (1978).
[10]J. E. A. Lys *et al.*, Phys. Rev. D 15, 1857 (1977); J. E. A. Lys, *ibid.* 16, 3127 (1977).
[11]G. Alberi, V. Hepp, L. P. Rosa, and Z. D. Thome, Nucl. Phys. B108, 327 (1976) and references cited therein.
[12]P. S. Eastman *et al.*, Nucl. Phys. B51, 29 (1973).
[13]P. D. Zemany, Z. Ming Ma, and J. M. Mountz, Phys. Rev. Lett. 38, 1443 (1977).
[14]J. M. Mountz, P. D. Zemany, and Z. Ming Ma (unpublished).
[15]R. Reid, Ann. Phys. (N.Y.) 50, 411 (1968).
[16]T. Hamada and I. D. Johnson, Nucl. Phys. 34, 382 (1962).
[17]S. Gartenhaus, Phys. Rev. 100, 900 (1955).
[18]L. Hulthen and M. Sugawara, Handb. Phys. 39, 141 (1957).
[19]M. Moravcsik, Nucl. Phys. 7, 113 (1958).
[20]I. J. McGee, Phys. Rev. 151, 772 (1966).
[21]A. Jurewicz and L. Satta, Lett. Nuovo Cimento 10, 217 (1974).
[22]B. Y. Oh and G. A. Smith, Nucl. Phys. B40, 151 (1972).
[23]E. Fermi, Phys. Rev. 81, 683 (1951).
[24]P. D. Zemany, Ph.D. thesis, Michigan State University, 1975 (unpublished).
[25]R. A. Donald *et al.*, Phys. Lett. 40B, 586 (1972); Nucl. Phys. B61, 333 (1973).
[26]W. A. Cooper *et al.*, Argonne National Laboratory report (unpublished).
[27]T. Handler *et al.*, Nucl. Phys. B101, 35 (1975); R. A. Donald *et al.*, *ibid.* B11, 551 (1969).
[28]N. Xuong and G. R. Lynch, Phys. Rev. 128, 1849 (1962).
[29]R. Burns *et al.*, Nucl. Phys. B27, 109 (1971).
[30]Liverpool-LPNHE (Paris) Collaboration, report submitted to XVI International Conference on High Energy Physics, Chicago and Batavia, Illinois, 1972 (unpublished).
[31]Z. Ming Ma., B. Y. Oh, D. L. Parker, and G. A. Smith, Phys. Lett. 47B, 177 (1973).
[32]A. Donnachie, R. G. Kirsopp, and C. Lovelace, CERN Report No. TH-838, 1967 (unpublished).